Theoretical study of electronic and optical properties of inverted $GaAs/Al_xGa_{1-x}As$ quantum dots with smoothed interfaces in an external magnetic field

V. Mlinar,[1,*] A. Schliwa,[2,3] D. Bimberg,[2] and F. M. Peeters[1]

[1]*Departement Fysica, Universiteit Antwerpen, Groenenborgerlaan 171, B-2020 Antwerpen, Belgium*

[2]*Institut für Festkörperphysik, Technische Universität Berlin, PN 5-2, Hardenbergstrasse 36, D-10623 Berlin, Germany*

[3]*Weierstrass Institute for Applied Analysis and Stochastics, Mohrenstr. 39, 10117 Berlin, Germany*

(Received 22 November 2006; revised manuscript received 7 February 2007; published 4 May 2007)

Magneto-optics of unstrained $GaAs/Al_xGa_{1-x}As$ quantum dots are investigated theoretically in the presence of an external magnetic field. Single-particle states, exciton binding energies, and the exciton diamagnetic shift are calculated with a confinement potential based on atomically resolved scanning tunneling microscopy pictures. The degree of interface intermixing is treated as a variable. The electronic structure of the dot in the presence of a magnetic field is calculated using eight-band $\mathbf{k}\cdot\mathbf{p}$ theory including a magnetic field. We find that varying interface roughness sensitively affects the interband but hardly the intraband energies. For magnetic fields applied both in the growth direction and perpendicular to it (for $B \leqslant 50$ T), we find good agreement between our predicted exciton diamagnetic shift and recent experimental magnetophotoluminescence data [N. Schildermans *et al.*, Phys. Rev. B **72**, 115312 (2005)]. The inherent coupling of valence and conduction bands taken into account in the eight-band $\mathbf{k}\cdot\mathbf{p}$ model explains well the observed experimental results.

DOI: 10.1103/PhysRevB.75.205308 PACS number(s): 73.21.La, 71.35.Ji

I. INTRODUCTION

The persistent interest in quantum dots (QDs) is driven by the multitude of their actual and potential applications ranging from novel lasers[1–3] and optical amplifiers[4] to physical representations of a quantum bit[5,6] or single polarized photon sources emitting "quantum bits."[7] The morphological properties of QDs grown by strained layer epitaxy strongly depend on the details of the growth conditions.[8,9] The occurrence of varying strain and piezoelectric fields in and around the dots and significant compositional intermixing lead to uncertainties in the determination of their geometry and composition, e.g., by high-resolution transmission electron microscopy.[1,9] Thus, the predictive power even of detailed theoretical models of electronic and optical properties[10–15] is limited by this uncertainty.

Recently, unstrained $GaAs/Al_xGa_{1-x}As$ QDs were fabricated through an ingenious multistep approach based on a combination of hierarchical self-assembly and *in situ* etching.[16] Photoluminescence (PL) of an ensemble of such QDs revealed an appreciably smaller inhomogeneous broadening, in the range of 8–15 meV depending on the growth conditions, indicating a good size homogeneity. The QDs have a typical lateral size of 35–65 nm and a thickness of ~6 nm.

Due to the nonexistence of strain and reduced uncertainties in the size and shape, such QDs represent an ideal test case for electronic structure models. In Ref. 16, an eight-band $\mathbf{k}\cdot\mathbf{p}$ model was successfully applied to describe the zero-field PL and single dot spectra. The zero-field PL measurements were subsequently extended to magnetic field up to 50 T by Schildermans *et al.*[17] and a single-band model modified to include conduction-band nonparabolicity[18] was implemented to describe the magnetic-field dependence.[19]

In the present paper, we extend the previous theoretical studies based on eight-band $\mathbf{k}\cdot\mathbf{p}$ theory[11] taking into account the effect of an external magnetic field.[20] Single-particle states, exciton binding energies, and its diamagnetic shift are calculated for magnetic fields applied in the growth direction as well as in the direction perpendicular to the growth direction. The calculations are based on a realistic confinement potential which is derived from high-resolution scanning tunneling microscopy (STM) data taken from Ref. 16. Recent cross-section scanning tunneling microscopy (X-STM) experiments demonstrate that the interfaces between GaAs and AlGaAs layers are not abrupt[21] as previously observed for quantum wells.[22] Since the size and shape of the dots are known, the previously not discussed effect[17,19] of this roughness on the electronic properties of the dots is investigated in detail.

This paper is organized as follows. Our theoretical approach is presented in Sec. II. The influence of interface intermixing on the transition energy is discussed in Sec. III. Section IV A contains an analysis of the electron, hole, and exciton energies as a function of the magnetic field treating interface roughness as a variable. In Sec. IV B, we compare our results with available experimental data. Finally in Sec. V, we discuss the question whether tunneling and conduction-band nonparabolicity induced by higher conduction bands have to be taken into account for explaining the experiments, as inferred by Ref. 19. Our results and conclusions are summarized in Sec. VI.

II. THEORETICAL APPROACH

Choice of the model QDs. The unique fabrication process used in Ref. 16 made it possible to extract the QD structure with great detail: Prior to the final step of QD deposition, the surface profile [see Fig. 1(a), red dotted line] has been scanned using STM while preserving the ultrahigh-vacuum conditions during epitaxy. The shape of the resulting QD is determined by this pattern and taken as the origin of our primary model QD. Next, a series of model QDs is derived from the primary one based on a systematic variation of

 ©2007 The American Physical Society

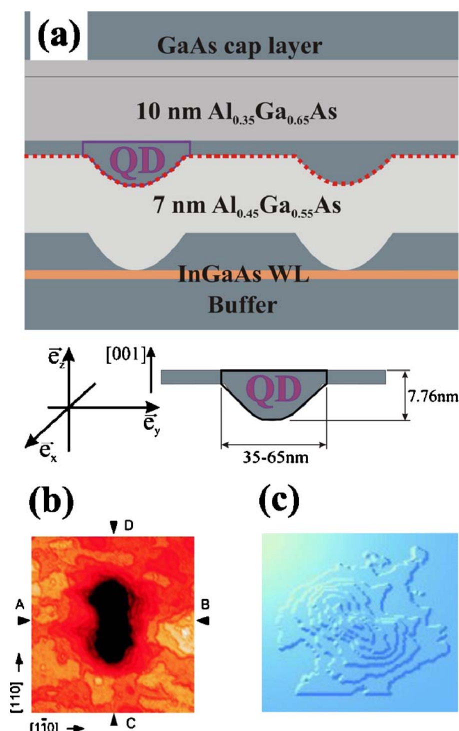

FIG. 1. (Color online) (a) Schematic sample structure of unstrained GaAs/AlGaAs quantum dots. The structure of the implemented model QD (c) is derived from STM measurements (b) taken from Ref. 16. The dotted line in (a) indicates the position where the STM picture is taken from.

Fickian diffusion induced interface roughness (see Fig. 2). The parameter N describes the degree of intermixing ($N=0$, no intermixing; $N=9$, strong intermixing). The parameter N is actually the number of smoothing steps at the interface. One smoothing step at one point of the grid describing the structure is taken as the average value of the material parameters of the structure on the neighboring points of the grid.

Electronic structure. The single-particle energies of our model QDs are extracted from an eight-band $\mathbf{k}\cdot\mathbf{p}$ Hamiltonian,[11] where the magnetic field is incorporated through standard Peierls substitution[23] in the wave-vector and Zeeman energy terms.[20] The parameters used for our structure are based on Γ-point band-structure parameters and

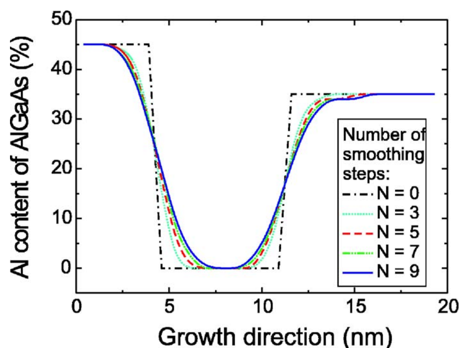

FIG. 2. (Color online) Vertical scan through the center of the model structures. The aluminum content is varied as a function of intermixing steps (N).

are given in Table I. The Hamiltonian is discretized on the three-dimensional (3D) rectangular grid (see Ref. 11), whereas the scheme is checked by testing its stability and consistency. Note that the computational error in our 3D calculations is of the order of several meV and results below this threshold were not discussed.

The excitonic states are calculated using the configuration-interaction method. The two-particle exciton Hamiltonian is expanded into a basis of antisymmetrized products of single-particle wave functions, thus accounting for direct Coulomb interaction and exchange. Correlation effects are accounted for by expanding the basis to include excited-state configurations.[24] The Coulomb and exchange matrix elements needed for the configuration-interaction (CI) calculation are computed numerically from six electron and six hole single-particle orbitals and are screened using different dielectric constants for GaAs and AlGaAs. Absorption is calculated by Fermi's golden rule applied to CI states. It is important to stress that no adjustable parameters are present in this model.

The experiments which we are referring to throughout this work were performed on an ensemble of QDs. When we compare our findings with the experimental results, we consider our model QD as representative for the ensemble of QDs. The latter is motivated by the unusual narrow photoluminescence broadening which points at an extremely homogeneous QD ensemble.

III. INFLUENCE OF INTERFACE INTERMIXING ON THE OPTICAL PROPERTIES

In a simplified picture, the carrier confinement in unstrained $GaAs/Al_xGa_{1-x}As$ QDs is only a function of the dot size and shape, where the conduction- and valence-band offsets are taken from those of the bulk materials. However, during the growth process Al-Ga intermixing at the interface is likely to occur, leading to changes of the aluminum/gallium content at the heterojunctions. Recently, obtained cross-section STM images of $GaAs/Al_xGa_{1-x}As$ QDs support this assumption, suggesting that interfaces of GaAs and AlGaAs layers are not abrupt.[21,22] Here, we investigate the consequences of such nonabrupt interfaces on the optical properties by treating the degree of interface intermixing as a variable.

In Fig. 2, a vertical scan through the center of the model structures is shown for different values of N, a quantity which parametrizes the degree of interface intermixing. The case $N=0$ corresponds to the ideal case of abrupt interfaces and $N=9$ to the case of strong interface intermixing. The corresponding local conduction and valence bands are shown in Figs. 3(a) and 3(c), and since they are extracted from the 3D rectangular grid, they show steplike profile. The interface smoothing leads to the increase of the QDs' effective size and to the decrease of the average Al content. As a consequence, the confinement of the electrons and holes is determined by two dominant effects present with increasing N: the first one is the effect of the increase of the QDs' size and the second one is the effect of the decrease of the average Al content.

TABLE I. Material parameters used for the electronic structure calculations.

Quantity	Unit	GaAs	AlAs	$Al_xGa_{1-x}As$
a	A	5.65	5.65	Linear
E_0	meV	1518.0	3060.0	$1518+1542x+x(x-1)(689x-18.5)$
E_v'	meV	−6920.0	−7377.0	$-6920-433x-24x^2$
Δ_0	meV	340.0	280.0	$340-131x+71x^2$
E_p	meV	25500.0	21100.0	$(1.132+0.758x)\frac{1-m_e}{m_e}\frac{3E_0(E_0+\Delta_0)}{3E_0+2\Delta_0}$
m_e	m_0	0.067	0.22	Linear
γ_1		7.1	4.04	$1/[(1-x)/7.1+x/4.04]$
γ_2		2.4	0.78	$1/[(1-x)/2.4+x/0.78]$
γ_3		2.91	1.57	$1/[(1-x)/2.91+x/1.57]$
ϵ_s		13.18	10.06	Linear
κ		1.28	0.12	Linear

Single-particle energies. The variation of the first three electron and hole energy levels with the number of intermixing steps is shown in Fig. 4. Two main results can be derived from this figure: First, Al-Ga intermixing leads to an increase of electron and hole energies and therefore to larger interband transition energies. Second, the electron intraband energies are almost unaffected by the interface roughening. The situation is similar for the hole intraband energies, except for N larger than 7, where the hole intraband energies slightly differ from those for smaller N. This behavior can be attributed to the increased confinement which leads to an enhanced valence-band mixing. Figures 3(b) and 3(d) show the lateral and vertical extent of the electron and hole ground state for the abrupt interface ($N=0$) and for the largest considered degree of intermixing ($N=9$): In both cases, the wave functions are more strongly localized for $N=9$. It means that the although the effective size of the quantum dot increases with increasing N, the decrease of the Al content with N is the dominant effect and it leads to the increased confinement for the electrons and holes. This result is different from the one reported in Ref. 25 for small InAs/GaAs QDs, where it was found that both carrier types tend to increase their wave-function extent upon annealing. The main reason for such a different behavior of electron (hole)-wave-function extent as a function of annealing can be found in the ratio between average QD size and electron (hole) Bohr radius, which is larger than 1 here and smaller than 1 in the case reported in Ref. 25.

Excitonic properties. As can be seen from Fig. 5, a change in the sharpness of the interfaces sensitively affects the exciton energy. The larger the N, the larger the exciton energy. We have already seen that the single-particle energies increase (Fig. 4) for higher values of N. The increase of electron and hole localization for larger interface intermixing, shown in Figs. 3(b) and 3(d), is also reflected by an increase of the exciton binding energy as illustrated in the inset of Fig. 5. Therefore, the increase of exciton energy upon interface intermixing is a result of the increased single-particle

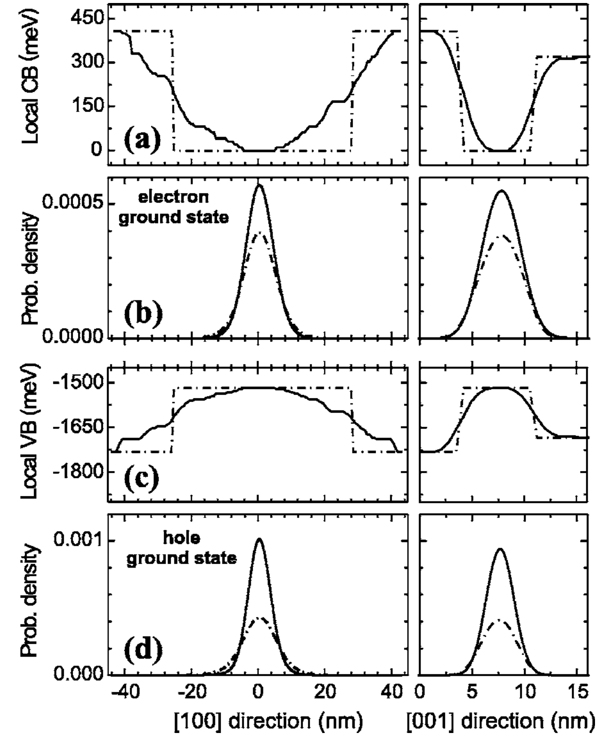

FIG. 3. Lateral (left) and vertical (right) scans through the local (a) conduction and (c) valence band edges of the model QD for $N=0$ (nonintermixed dashed) and $N=9$ (strongly intermixed). The respective square moduli of electron and hole wave functions are shown in (b) and (d), respectively. The lateral scans through the confinement potential and the probability density are taken at a vertical position 1 nm below the GaAs quantum well (average of the z component of the wave-function barycenter). Since the potential width is determined at this upper z position, it appears large compared to the lateral-wave-function extent. The steplike lateral confinement potential after annealing [(a) and (c)] originates from a combination of the terracelike QD structure and the applied smoothing procedure.

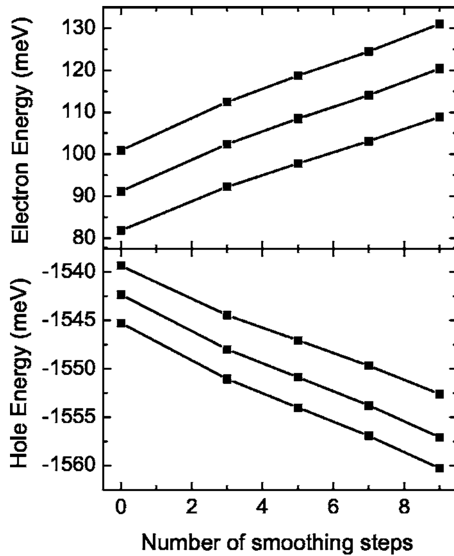

FIG. 4. The variation of the first three electron and hole energy levels as a function of N.

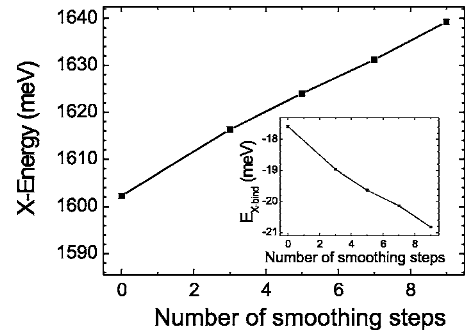

FIG. 5. Exciton energy as a function of the number of smoothing steps. The inset shows the exciton binding energy as it varies with the number of smoothing steps.

energies, resulting in a stronger wave-function localization. Figure 6 finally shows the calculated excitonic absorption spectra as a function of N.

A comparison to measured single-QD PL spectra[16] yields very good agreement for an intermixing value of $N=3$. With increasing N, a blueshift of the whole spectrum occurs (37 meV between $N=0$ and $N=9$), whereas the distances between the peaks remain approximately the same.

IV. PRESENCE OF AN EXTERNAL MAGNETIC FIELD

In this section, we explore the behavior of electron, hole, and exciton energies as a function of magnetic field. Both cases of a magnetic field applied parallel as well as perpendicular to the growth direction are considered. Excitonic absorption spectra are calculated for different values and orientations of B and as a function of the degree of interface intermixing. Finally, we compare our theoretical findings for the exciton diamagnetic shift to experimental results from Ref. 17.

A. Role of the magnetic-field direction

Single-particle energies. An external magnetic field introduces an additional confinement in the plane perpendicular to the field direction of the applied field and lifts the Kramers degeneracy. Its impact on the electronic properties depends on the strength of the already existing QD confinement. It is large for small confinement and small for large confinement. Since our QDs are very flat, the confinement is strong in the growth direction ($\mathbf{e}_z$) and weak in the lateral direction. Therefore, we expect a large effect if the B field is applied parallel to $\mathbf{e}_z$ and a smaller one if applied perpendicular to $\mathbf{e}_z$. The results of the corresponding calculations are shown in Fig. 7.

For the case of a lateral magnetic field, the strong QD confinement in the growth direction limits the influence of the magnetic field. In contrast, for the case of a magnetic field applied in the growth direction, electron and hole energy levels are strongly influenced by the magnetic field and a magnetic-field-induced band mixing of the hole energy levels is observed. This is a direct consequence of the relatively smaller lateral confinement in the dot (e.g., magnetic length for $B=10$ T is about 8 nm, while the base length of the dot is about 35 nm). Electron and hole wave functions for the two different magnetic-field orientations are also shown in Fig. 7. One can clearly see the impact of the additional lateral confinement for $\mathbf{B}\parallel\mathbf{e}_z$ on the lateral electron- and hole-wave-function extent, which does not occur for $\mathbf{B}\parallel\mathbf{e}_x$. An exchange of the character of the hole wave functions for magnetic field of $B=20$ T applied in the growth direction is clearly observed. For $B\approx 17$ T, the h_0 energy level anticrosses with the h_1 level. As a consequence, the hole wave function that corresponds to the h_0 energy level before the anticrossing is h_1-wave-function-like after anticrossing (see hole wave functions in Fig. 7), whereas the wave function that corresponds to h_1 energy level before anticrossing is h_0-wave-function-like after the anticrossing.

Role of the interface roughness. In Sec. III, we demonstrated that the interface intermixing increases the localization of the electrons and holes. As a consequence, it leads to the reduced influence of the magnetic field on the electrons and holes. It is therefore clear that the increase of the parameter N leads to an even smaller dependence of the electron and hole energy levels for lateral magnetic field, while for a

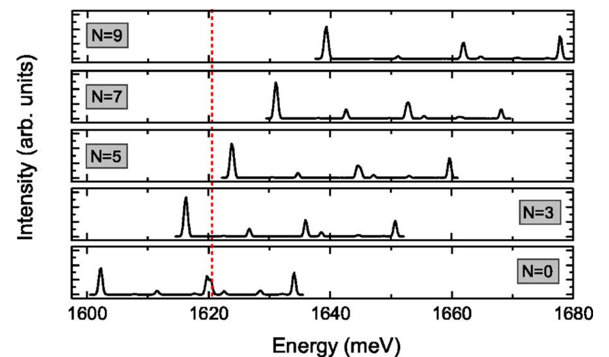

FIG. 6. (Color online) Exciton absorption spectra as a function of N. A blueshift in the transition energy with increasing interface intermixing is observed. The vertical dotted line indicates the position of the measured PL peak.

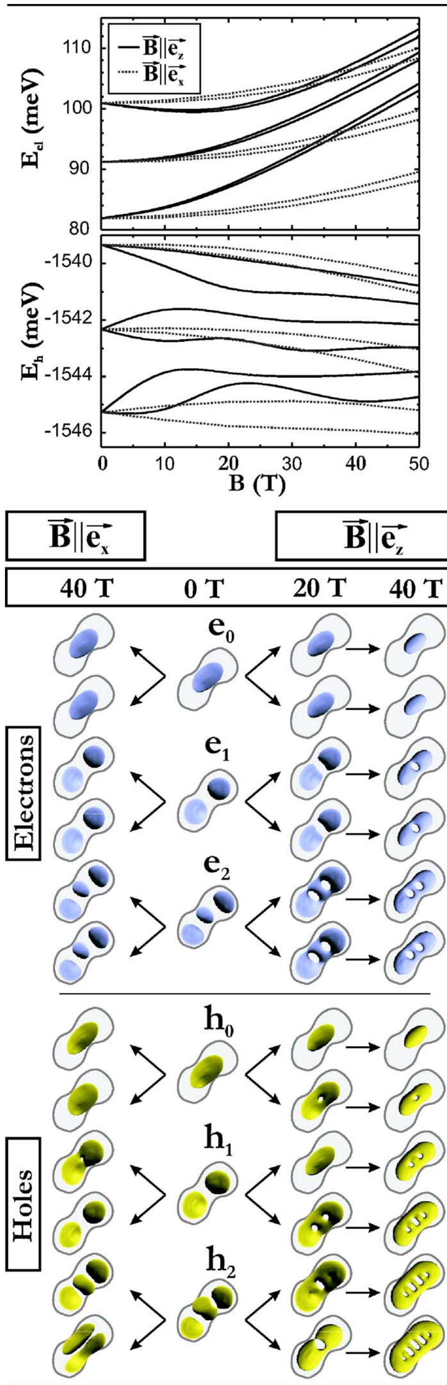

FIG. 7. (Color online) Electron and hole energy levels (with respect to the GaAs conduction band) as a function of the magnetic field parallel to the growth direction (black lines) and perpendicular to the growth direction (light gray lines) are shown. The case of for an ideal sharp interface ($N=0$) is shown. The wave-function isosurfaces are plotted for 65% probability density.

vertical magnetic field of variation of N does not lead to the significant changes of the electron and hole energy levels with magnetic field. These conclusions are illustrated in Table II for both directions.

Exciton binding energy. The magnetic-field dependence

TABLE II. The shift of the electron and hole energies as a function of N for two different magnetic-field directions.

	ΔE_e(40 T) (meV)		ΔE_h(40 T) (meV)	
N	$\mathbf{B}\parallel\mathbf{e}_z$	$\mathbf{B}\parallel\mathbf{e}_x$	$\mathbf{B}\parallel\mathbf{e}_z$	$\mathbf{B}\parallel\mathbf{e}_x$
0	15.26	6.22	−1.45	−0.69
3	13.85	3.5	−0.14	−0.4
5	13.19	3.5	−0.14	−0.4
7	8.7	3.25	−0.99	−0.2
9	8.03	3.16	−0.96	−0.11

of the exciton binding energy is analyzed by considering the quantity $\Delta E_{X\text{-}bind}$ defined as

$$\Delta E_{X\text{-}bind} = E_{X\text{-}bind}(B) - E_{X\text{-}bind}(B=0),$$

with $E_{X\text{-}bind}(B)$ being the exciton binding energy at magnetic field B. In Fig. 8, $\Delta E_{X\text{-}bind}$ is shown as a function of the B field and its orientation and the degree of interface intermixing. Since the magnetic field further enhances the wave-function localization, it is of no surprise that the exciton binding energies $E_{X\text{-}bind}$ increase upon an increase of the magnetic field [see Fig. 8(a)]. This effect is much larger for $\mathbf{B}\parallel\mathbf{e}_z$ than for $\mathbf{B}\parallel\mathbf{e}_x$ since in the former case the increase of the wave-function localization is much stronger than in the latter. As the interface smoothing leads to an additional carrier localization in our case, $\Delta E_{X\text{-}bind}$ becomes smaller as a function of N [see Fig. 8(b)].

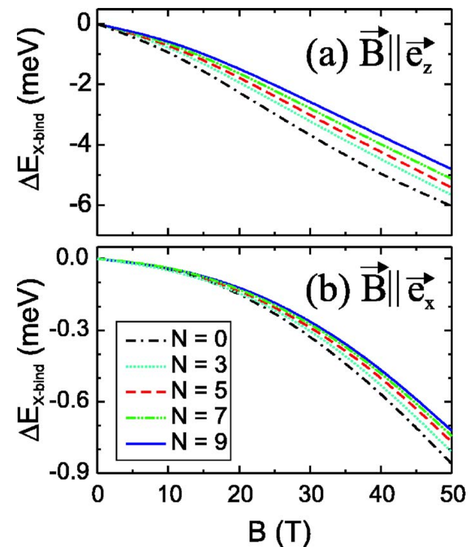

FIG. 8. (Color online) Exciton binding energies as a function of magnetic field applied (a) in the growth direction and (b) in the direction perpendicular to the growth direction for different interface intermixing. $\Delta E_{X\text{-}bind}$ defined as $\Delta E_{X\text{-}bind}=E_{X\text{-}bind}(B) - E_{X\text{-}bind}(B=0)$, where $E_{X\text{-}bind}(B)$ is exciton binding energy for value of magnetic field B, and $E_{X\text{-}bind}(B=0)$ is exciton binding energy in the absence of a magnetic field.

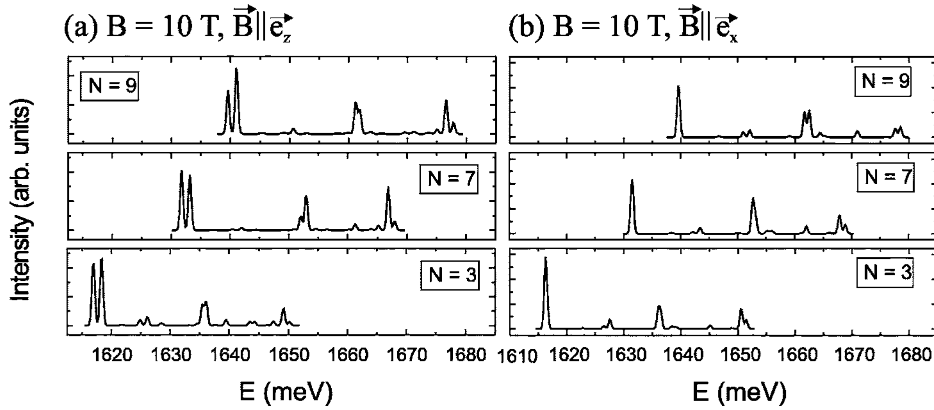

FIG. 9. Exciton absorption spectra for $B=10$ T applied in the growth direction for three values of N, $N=3,7,9$.

The effect of smoothing of the interface on the excitonic absorption spectra for $B=10$ T for magnetic field applied in the growth direction and in plane is shown/illustrated/depicted in Figs. 9(a) and 9(b), respectively. The exciton absorption spectra are richer for the case of magnetic field applied in the growth direction. The reason for this can be found in the larger spin splitting and the arising additional transitions in a magnetic field whose effect on the electronic structure is much larger than in the case of magnetic field applied in plane.

B. Comparison with experiment

The exciton absorption spectrum of our model QD for $N=3$ has already shown excellent agreement with the measured single-QD PL and photoluminescence excitation (PLE) spectra[16] in the absence of an external magnetic field. In Ref. 17, the same samples have been used to perform low and high excitation PL measurements using high magnetic fields parallel and perpendicular to the growth direction. In Figs. 10 and 11, we compare the excitonic absorption spectra to the high exciton PL results for both field directions. Although the latter case corresponds to a multiexcitonic decay rather than excitonic absorption, we can link the p-p channel absorption to the decay of three- and fourfold excitons and the d-d channel absorption to that of the five- and sixfold excitons, provided the renormalization effects, being linked to the presence of more than one exciton, are small. The agreement, however, is quite remarkable: Our calculations reproduce the experimental results qualitatively and to a large degree also quantitatively.

The splitting of the s-s channel peaks, caused by the Zeeman splitting of the single-particle orbitals, is smaller than the experimental PL broadening and therefore hidden in the experimental data. The smaller splitting of these peaks for lateral magnetic field is related to the smaller Zeeman splitting of electron and hole orbitals, which in turn is related to the large z confinement. An explanation for such a behavior of the exciton absorption spectra as a function of the orientation of a magnetic field is given in Sec. IV A.

Exciton diamagnetic shift. More information about the interplay between the Coulomb interaction and the QD confinement in the direction perpendicular to the direction of the

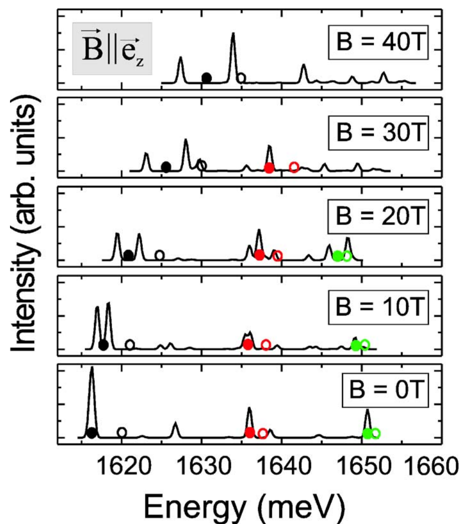

FIG. 10. (Color online) Comparison between calculated excitonic absorption spectra ($N=3$) and the measured peak positions in the high excitation PL spectra (open symbols). The bold symbols are guide to the eyes. The experimental values are taken from a QD sample with a slightly thicker AlGaAs barrier, leading to a shallower QD compared to our model QD.

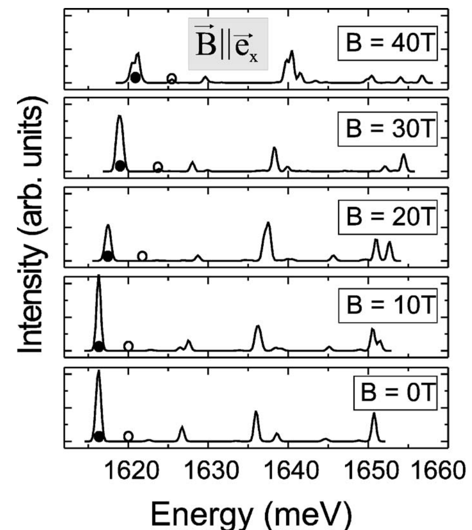

FIG. 11. The same as Fig. 10 but now for magnetic field applied in the lateral direction. The available experimental data are shown by open symbols.

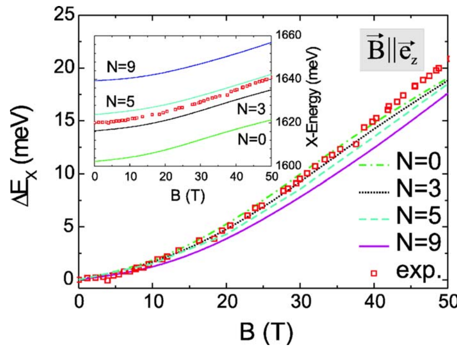

FIG. 12. (Color online) The exciton diamagnetic shift as the function of a magnetic field for the optical active exciton states compared to the experimental results (symbols). An external magnetic field is applied in the growth direction. The inset depicts the absolute values for the calculated exciton energy vs magnetic field together with the experimental data.

applied magnetic field can be obtained by considering the exciton diamagnetic shift defined as

$$\Delta E_{exc} = E_{exc}(B) - E_{exc}(B = 0 \text{ T}).$$

The transition energies of two lowest-lying optically active excitons are averaged since their Zeeman splitting is smaller than the broadening of the PL. The obtained data for the exciton diamagnetic shift are compared to the position of the PL peak taken from Ref. 17 for both orientations of the magnetic field and for different values of N of the interface intermixing. The best agreement for the diamagnetic shift for both magnetic-field directions is achieved for a value of N between 0 and 3, whereas for the absolute values of E_X (see inset of Figs. 12 and 13) the agreement is best for N values between 3 and 5.

Furthermore, as can be seen from Fig. 8, a smoother interface does not significantly affect the change of the exciton binding energy with magnetic field. The changes in the curvature of the exciton diamagnetic shift with the variation of N from 0 to 3 or from 3 to 5 are not significant when the magnetic field is applied in the growth direction, as shown in Fig. 12, and good agreement with the experimental data is achieved for all these values of N ($N=0,3,5$). A significant discrepancy to the experimental data is only observed if N is

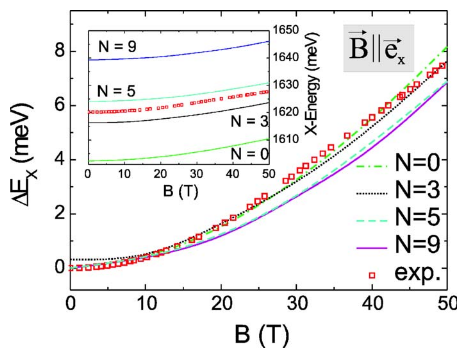

FIG. 13. (Color online) The same as Fig. 12 but now for magnetic field applied in the lateral direction.

larger than 5. For the lateral-magnetic-field case, one can see from Fig. 13 that the relative exciton diamagnetic shift for $N=5$ is quite close to that for $N=9$. This is related to the increased vertical QD confinement for $N \geqslant 5$, which leads to a suppression of the magnetic-field influence (magnetic length is larger than the height of the dot). The best overall agreement between our findings on the exciton energy and the exciton diamagnetic shift with the experimental data is obtained for our model QD with $N=3$. This result is in perfect agreement with the reported experimental results of Ref. 21 obtained from X-STM measurements on samples fabricated by using the same growth mode.

A similar comparison has been recently performed[19] using a single-band model with additional terms for the conduction-band nonparabolicity. Good agreement for the relative exciton shift was obtained, whereas the absolute PL energies were not reproduced accurately. Note that the electron effective mass dominates in the exciton effective mass, and therefore any changes in the electron effective mass would be directly reflected through the changes in the relative exciton shift. Therefore, as the main stumble point in the approach of Ref. 19 arises the question of the degree of the conduction-band nonparabolicity actually present in the system. It was *a priori* assumed to increase, originating from coupling to higher conduction bands. Based on the eight-band $\mathbf{k}\cdot\mathbf{p}$ model, we showed here that the inherent coupling of valence and conduction bands present in the eight-band $\mathbf{k}\cdot\mathbf{p}$ model is sufficient for explaining the effects observed in Ref. 17 without additional nonparabolicity induced by coupling to higher-lying conduction bands.

V. DISCUSSION

First, the interdiffusion of aluminum at the heterojunction during the growth significantly influences the transition energies (see Sec. III). The ground-state transition energies for the ideal case of no intermixing ($N=0$ in Fig. 6) and the case of strong intermixing ($N=9$ in Fig. 6) differ by about 37 meV, while interlevel transitions are not affected significantly. For example, for $N=0$ the distance between transition 1 and transition 2 is 9.2 meV, while in the case of $N=9$ this distance is 11.8 meV. The observed blueshift between PLE data and calculated absorption spectrum extracted from eight-band $\mathbf{k}\cdot\mathbf{p}$ theory[16] can be explained by this intermixing. The effect of interface intermixing is far from being negligible and should be properly taken into account for potential applications of these systems in optoelectronic devices.

Second, the influence of an applied external magnetic field in the growth direction as well as in plane on the electronic and optical properties was studied in Sec. IV. In general, since the dots are quite large in the lateral direction, the effect of a magnetic field applied in the growth direction is more pronounced than if the magnetic field is applied perpendicular to the growth direction. For example, complicated behavior of hole energy levels as a function of magnetic field applied in the growth direction with strong anticrossing does not exist in the case of magnetic field applied perpendicular to the growth direction, which is a direct consequence of the

competition between the confinement and magnetic field.

Two questions were raised in Ref. 17 related to tunneling and the degree of nonparabolicity of the conduction band and its influence on the excitonic properties. In our model, we explicitly include the mixing of the lowest-lying conduction band and the three topmost valence bands. Next, in the modeling of the excitonic properties, the direct Coulomb interaction, exchange, and correlation were included. From Figs. 3(b) and 3(d), it is clear that the penetration of the electron and hole wave functions into the barrier is small and that interface intermixing even increases the localization of the electrons and holes. Therefore, we conclude that the effect of tunneling in these structures is negligible.

The nonparabolicity of the conduction band originates from the coupling to the valence band and to higher conduction bands. In our eight-band $\mathbf{k}\cdot\mathbf{p}$ model, only the former is accounted for. The confinement and hence the localization of electron and hole states comes into play due to their resulting spread in k space, and the accompanying contributions far from the Γ point. This confinement in our case comes predominantly from the dot itself and is enhanced by the applied magnetic field.

From Figs. 10–13, it is clear that our fit-parameter-free results agree very well with the experimental data. We conclude that the inherent coupling of valence and conduction bands present in the eight-band $\mathbf{k}\cdot\mathbf{p}$ model is sufficient for explaining the effects observed in Ref. 17 without additional nonparabolicity originating form coupling to higher conduction bands.

VI. SUMMARY AND CONCLUSIONS

We studied the electronic structure of unstrained $GaAs/Al_xGa_{1-x}As$ QDs in the presence of an external magnetic field. Interface roughness was observed to sensitively affect the transition energies, but hardly the intraband energies. For a magnetic field applied in the growth direction and in the direction perpendicular to the growth direction (where $B \leq 50$ T), we find good agreement between the exciton diamagnetic shift obtained from our calculations and the experimental data from Ref. 17. We discussed the effect of tunneling and the degree of nonparabolicity and found that tunneling was negligible in our model and that inherent coupling of valence and conduction bands present in the eight-band $\mathbf{k}\cdot\mathbf{p}$ model is sufficient to explain the "nonparabolicity" effects reported in Ref. 17.

ACKNOWLEDGMENTS

We acknowledge fruitful discussion with Oliver Stier and Armando Rastelli. This work was supported by the Belgian Science Policy, TOP-BOF (University of Antwerp), and the European Union Network of Excellence: SANDiE. The electronic structure calculations were performed using the IBM pSeries Supercomputer of the HLRN (Berlin and Hannover) and the authors thank all members of the HLRN for their support.

*Electronic address: vladan.mlinar@ua.ac.be

[1] D. Bimberg, M. Grundmann, and N. N. Ledentsov, *Quantum Dot Heterostructures* (Wiley, Chichester, 1998); D. Bimberg and N. N. Ledentsov, J. Phys.: Condens. Matter **15**, R1063 (2003).

[2] F. Heinrichsdorff, Ch. Ribbat, M. Grundmann, and D. Bimberg, Appl. Phys. Lett. **76**, 556 (2000); Y. M. Manz, A. Christ, O. G. Schmidt, T. Riedl, and A. Hangleiter, *ibid.* **83**, 887 (2003).

[3] J. Tatebayashi, N. Hatori, M. Ishida, H. Ebe, M. Sugawara, Y. Arakawa, H. Sudo, and A. Kuramata, Appl. Phys. Lett. **86**, 053107 (2005).

[4] A. V. Uskov, E. P. O'Reilly, R. J. Manning, R. P. Webb, D. Cotter, M. Laemmlin, N. N. Ledentsov, and D. Bimberg, IEEE Photonics Technol. Lett. **16**, 1265 (2004).

[5] F. Troiani, E. Molinari, and U. Hohenester, Phys. Rev. Lett. **90**, 206802 (2003); F. Troiani, J. I. Perea, and C. Tejedor, Phys. Rev. B **73**, 035316 (2006).

[6] D. P. DiVincenzo, Science **270**, 255 (1995); D. Loss and D. P. DiVincenzo, Phys. Rev. A **57**, 120 (1998); A. Imamoglu, D. D. Awschalom, G. Burkard, D. P. DiVincenzo, D. Loss, M. Sherwin, and A. Small, Phys. Rev. Lett. **83**, 4204 (1999).

[7] O. Benson, C. Santori, M. Pelton, and Y. Yamamoto, Phys. Rev. Lett. **84**, 2513 (2000).

[8] S. T. Stoddart, A. Polimeni, M. Henini, L. Eaves, P. C. Main, R. K. Hayden, K. Uchida, and N. Miura, Appl. Surf. Sci. **123/124**, 366 (1998); J. Maes, M. Hayne, V. V. Moshchalkov, A. Patanè, M. Henini, L. Eaves, and P. C. Main, Appl. Phys. Lett. **81**, 1480 (2002); S. Godefroo, J. Maes, M. Hayne, V. V. Moshchalkov, M. Henini, F. Pulizzi, A. Patanè, and L. Eaves, J. Appl. Phys. **96**, 2535 (2004).

[9] V. A. Shchukin and D. Bimberg, Rev. Mod. Phys. **71**, 1125 (1999); V. A. Shchukin, N. N. Ledentsov, and D. Bimberg, *Epitaxy of Nanostructures* (Springer, Berlin, 2003).

[10] M. Grundmann, O. Stier, and D. Bimberg, Phys. Rev. B **52**, 11969 (1995).

[11] O. Stier, M. Grundmann, and D. Bimberg, Phys. Rev. B **59**, 5688 (1999).

[12] L. He, G. Bester, and A. Zunger, Phys. Rev. Lett. **94**, 016801 (2005).

[13] G. A. Narvaez, G. Bester, and A. Zunger, Phys. Rev. B **72**, 245318 (2005).

[14] V. Mlinar, M. Tadić, and F. M. Peeters, Phys. Rev. B **73**, 235336 (2006); M. Tadić, V. Mlinar, and F. M. Peeters, Physica E (Amsterdam) **26**, 212 (2005).

[15] V. Mlinar and F. M. Peeters, Appl. Phys. Lett. **89**, 261910 (2006).

[16] A. Rastelli, S. Stufler, A. Schliwa, R. Songmuang, C. Manzano, G. Costantini, K. Kern, A. Zrenner, D. Bimberg, and O. G. Schmidt, Phys. Rev. Lett. **92**, 166104 (2004).

[17] N. Schildermans, M. Hayne, V. V. Moshchalkov, A. Rastelli, and O. G. Schmidt, Phys. Rev. B **72**, 115312 (2005).

[18] U. Ekenberg, Phys. Rev. B **40**, 7714 (1989).

[19] Y. Sidor, B. Partoens, F. M. Peeters, N. Schildermans, M. Hayne, V. V. Moshchalkov, A. Rastelli, and O. G. Schmidt, Phys. Rev. B **73**, 155334 (2006).

[20] V. Mlinar, M. Tadić, B. Partoens, and F. M. Peeters, Phys. Rev. B **71**, 205305 (2005).

[21] A. Lenz, R. Timm, H. Eisele, L. Ivanova, D. Martin, V. Vosse-

burger, A. Rastelli, O. G. Schmidt, and M. Dähne, Phys. Status Solidi B **243**, 3976 (2006).

[22] M. A. Hermann, D. Bimberg, and J. Christen, J. Appl. Phys. **70**, R1 (1991).

[23] J. M. Luttinger, Phys. Rev. **102**, 1030 (1956).

[24] S. Rodt, A. Schliwa, K. Pötschke, F. Guffarth, and D. Bimberg, Phys. Rev. B **71**, 155325 (2005).

[25] R. Seguin, A. Schliwa, T. Germann, T. Hammerschmidt, S. Rodt, K. Pötschke, U. Pohl, P. Kratzer, and D. Bimberg Appl. Phys. Lett. **89**, 263109 (2006).